Simulations of the temperature dependence of energy transfer in the PSI core antenna

Yiwei Jia, John M. Jean,* Melanie M. Werst, Chi-Kin Chan, and Graham R. Fleming
Department of Chemistry, and the James Franck Institute, The University of Chicago, Chicago, Illinois 60637 USA; and
*Department of Chemistry, Washington University, St. Louis, Missouri 63130-4899 USA

ABSTRACT In order to understand the organization of the PSI core antenna and to interpret results obtained from studies of the temperature and wavelength dependence of energy transfer and trapping in the PSI particles, we have constructed a model for PSI in which spectral heterogeneity is considered via a self-consistent approach based on Forster transport. The temperature dependence of the absorption and emission spectra of the individual Chl molecules in the protein matrix is calculated based on a model Hamiltonian which includes a phonon contribution. Time and wavelength resolved kinetics of PSI at different temperatures are investigated by means of two-dimensional lattice models. We conclude that wavelength-dependent fluorescence decay kinetics result only when two or more bottlenecks exist in the energy transfer and trapping process. A single trap or several pseudo-traps with spectrally identical environments do not lead to wavelength dependent decays. Simple funnel arrangements of the spectral types can be ruled out. At least one pigment with energy lower than the photochemical trap located close to the reaction center is required to produce the trends of the fluorescence lifetimes observed experimentally. The remainder of the core antenna is consistent with a random arrangement of spectral types.

INTRODUCTION

A complete description of energy transfer and trapping in the light harvesting process is a formidable task. It can be approached at a variety of levels from the description of energy transfer between a single pair of antenna molecules up to the organization and operation of the entire antenna system. Difficult and unanswered questions remain at all levels of description. For example, little is known at the molecular level about the organization of the antenna, although the recent work of Kuhlbrandt and Wang (1991) on the light harvesting complex II (LHCII) is an important step forward. However, it is important to note that even very detailed structural information will not necessarily allow a complete picture of the dynamics. A major reason for this is that the protein perturbs the electronic states of the chlorophyll (Chl) molecules quite significantly both through "solvent shifts" and through conformational distortion (Gudowska-Nowak et al., 1990). For example, in the antenna complex of *Prosthecochloris aestuarii* (*P. aestuarii*) Gudowska-Nowak et al. (1990) find that the Q_y transition energies of the bacteriochlorophyll (BChl) molecules vary by up to 2,700 cm^{-1} as a result of interactions with the protein. Clearly, such large shifts will greatly influence the details of energy transfer no matter what the microscopic mechanism is. For the crudest model of energy flow in which the actual structure is used it is necessary to know which molecule absorbs at which wavelength. Despite the fact that structural information has been available on this protein for over fifteen years no completely satisfactory calculation of its absorption and circular dichroism spectra is yet available (Pearlstein, 1991).

For descriptions on the largest scale a number of "low resolution" approaches have been used. Initially, kinetic schemes were developed by Butler (1975a, 1975b) and have been exploited more recently by Holzwarth and co-workers (1986, 1987, 1989, and 1991), Wittmershaus (1987), and Mukerji and Sauer (1989). Analytical regular lattice models were developed by Pearlstein (1982; Hemenger et al., 1972) and used with some success on photosystem-I core particles by Owens et al. (1987, 1988, and 1989). In order to explore issues of spatial and spectral inhomogeneity, numerical versions of the lattice model were studied by Jean et al. (1989) and Pullerits and Freiberg (1991). In all these approaches the spatial characteristics of the antenna are considered at various levels of approximation but the couplings between the molecules are taken as empirical parameters. On the more microscopic level, Small and co-workers (Gillie et al., 1989) and Lyle and Struve (1991) have modeled the temperature dependence of a single energy transfer step using multiphonon radiationless transition theory (Jortner, 1976). In these calculations no attempt was made to consider the influence of spatial and spectral heterogeneity in the antenna as a whole. At the microscopic level many challenging questions exist. Can energy flow be described by weak coupling theory (Forster, 1965), strong coupling theory (Forster, 1965), or a mixture of the two as the result of weak coupling between groups of strongly coupled chromophores (Lyle and Struve, 1991)? At any level of description, what is the role of protein modes (phonons)? Can vibrational dephasing be assumed to be fast on the time scale of the energy transfer? Studies of the temperature dependence of energy transfer should shed light on a number of these questions. To date, however, the experimental situation is not especially clear. Small and co-workers (Gillie et al., 1989; and Lyle and Struve, 1991) have concluded, from studies of photosystem I preparations that contain both core and peripheral antenna (PSI-200), that energy transfer is very slow at low temperature (e.g., 300 ps at 1.6 K). By contrast, van der Laan et al. (1990) find that

0006-3495/92/07/259/15 $2.00

energy transfer in the antenna of *Rhodobacter sphaeroides* (*R. sphaeroides*) is rapid and shows little temperature dependence between 1.2 and 30 K. In addition, energy migration within the bacterial reaction center is still unresolvably rapid at 10 K (Breton et al., 1988).

We have recently completed a study of the temperature dependence of energy transfer and trapping in PSI core particles (40–50 Chl *a*/P700) and in whole cells of a PSI-only mutant (Werst et al., 1992). Fluorescence decay measurements on whole cells and PSI core particles of the PSI-only mutant of *Chlamydomonas reinhartii,* A4d, show that a short component (15–80 ps) dominates the kinetics (Werst et al., 1992). Owens et al. (1988) showed that P700 activity is directly correlated with the amplitude of the short component. Whole cells of A4d contain 60–70 Chl *a*/P700 and an additional 60–70 Chl $a + b$ from light harvesting proteins. For whole cells the short component monitored at emission wavelengths 680, 690, 700, and 710 nm shows little temperature dependence in the range 36–295 K. The lifetimes monitored at 680 and 690 nm decrease from 40–50 ps at 295 K to 20–30 ps at 36 K. The lifetimes monitored at 700 and 710 nm show negligible change over this temperature range (~30 and 50 ps, respectively). However, the lifetime of the short component monitored at 720 nm increases appreciably over this temperature range from 40 ps at 295 to ~110 ps at 30 K. For PSI particles (40–50 Chl *a*/P700), the short lifetimes for all emission wavelengths 680, 690, 700, 710, and 720 nm are in the range of 15–25 ps at room temperature. The emission monitored at 680 and 690 nm shows little temperature dependence from 10–20 ps in the range 36–295 K. However, the lifetimes of the short components monitored at 700, 710, and 720 nm all increase from ~20 ps at 295 to 45, 70, and 80 ps at 36 K, respectively. These data form the basis of our criterion for excluding models of the PSI core antenna. This paper is an attempt to deal with a number of the issues raised above and provide a description of our data which sheds light on the structure of the core PSI antenna system.

Many factors are clearly relevant in the temperature dependence of energy transfer and trapping. In considering the microscopic details of energy transfer two factors seem of particular significance: the temperature dependence of the spectral overlaps, and the role of Boltzmann factors in controlling the rates of "uphill" transfers. A major goal of this paper is to consider the competition between these two factors. The role of low energy (red) pigments (if such species exist) in focusing energy to the reaction center has been discussed (van Grondelle et al., 1988) and it appears that our time and wavelength resolved data (Werst et al., 1992) are particularly suited to an examination of these issues.

Our starting point is the absorption spectrum of the system. The availability of a very detailed set of Frank-Condon factors for Chl *a* in PSI (Gillie et al., 1989), and of modern matrix methods to calculate spectra with many degrees of freedom (Friesner et al., 1985; Munn and Silbey, 1978), given a model Hamiltonian, allow the "first principles" calculation of the absorption and emission spectra of individual Chl molecules in the protein matrix. Coupling to a low frequency phonon mode is included and thus (at a certain level of approximation) all homogeneous spectral broadening mechanisms are explicitly included in the Hamiltonian (Harris et al., 1986). Thus, the temperature dependence of the spectral width of a given Chl molecule can be calculated without further input. In this approach the spectral broadening arises from the thermal population of the low frequency modes. In order to model the in vivo spectrum we must consider the effects of inhomogeneous broadening (or diagonal disorder). It is not obvious whether a continuous distribution of transition energies or a set of discrete spectral types (each with some inhomogeneous width) is the more appropriate description. Gaussian deconvolution of antenna absorption spectra has been a routine practice (Ikegami, 1983; Ikegami and Itoh, 1988; Jennings et al., 1990; Owens et al., 1988) and the use of spectral types has become common. Some support for this approach comes from the molecular orbital calculations of Gudowska-Nowak et al. (1990), where large (up to 2,700 cm^{-1}) shifts in transition energies as a result of pigment–protein interactions are calculated for BChl *a* molecules in the antenna complex of *P. aestuarii.* Our approach is to use a combination of spectral types (typically 5–7 plus P700) each with a temperature independent 200-cm^{-1} inhomogeneous spectral width which is taken from the hole-burning work of Small and coworkers (Hayes et al., 1988). With this model, the absorption spectrum of the entire model antenna can then be calculated under the further assumption of weak coupling between the antenna chromophores.

Given the temperature dependence of the spectral properties of the various spectral types we then investigate energy migration and the time and wavelength resolved kinetics by means of two-dimensional lattice models using the methods developed by Jean et al. (1989). If energy transfer is assumed to occur by the Forster mechanism all that is required is the spatial arrangement and temperature dependent spectral overlaps. Thus, the calculation is self consistent in the weak coupling limit.

Of particular interest in our simulations is the existence of the red pigments (pigments that absorb at a wavelength longer than the reaction center (RC) absorption maximum), the temperature dependence, and wavelength dependence of energy transfer in the PSI core antenna. If the red pigments do exist, we expect the locations of these low energy sites to play an important role in the energy transfer in the PSI core antenna.

CALCULATION OF ABSORPTION SPECTRA

In this section we discuss calculations of the absorption spectrum of PSI based on a microscopic model of the

single site optical spectrum of a Chl-protein complex. With the absorption and emission lineshapes of a single spectral type in hand, the assumption of weak excitonic coupling between chromophores allows us to calculate the Förster rate for excitation transfer between any pair of Chls via integration of the spectral overlap.

(a) Temperature dependence of the single spectral type absorption and emission spectra

Our model for the ground and excited state potential surfaces for a Chl *a* molecule bound to a protein is based on the nonphotochemical hole-burning results of Small and co-workers (Gillie et al., 1989) who measured linear displacements between ground and excited states for 41 Frank-Condon active modes of Chl. In addition, their results also showed coupling of the S_0–S_1 transition to a narrow phonon band of mean frequency 22 cm^{-1}. The coupling to the phonon mode was found to be considerably stronger than coupling to any of the intramolecular modes, suggesting that this mode may be important in the intermolecular energy transfer dynamics. Thermal population of this mode results in significant line broadening of the Chl *a* vibronic spectra. In a time domain view, the optical dephasing rate of the intramolecular energy transitions receives a considerable contribution from the electron–phonon coupling to the low frequency phonon mode. In order to accurately investigate the temperature dependence of the absorption and emission spectra of a single spectral type of Chl *a*, we adopt the matrix method developed by Friesner et al. (1985). This is a time-domain approach that yields the exact thermally averaged transition dipole autocorrelation function assuming harmonic surfaces. The optical lineshape is recovered via numerical Fourier transform. The advantage of this type of approach is that we circumvent the need for determining the eigenvalues and eigenvectors of the excited state Hamiltonian. The total Hamiltonian for the two electronic state system is

$$H = H_0(q)|0\rangle\langle 0| + H_1(q)|1\rangle\langle 1|, \tag{1}$$

where q represents the full set of Franck-Condon modes and 0 and 1 denote the ground and excited electronic states, respectively. We assume the ground and excited state vibrational Hamiltonians, $H_0(q)$ and $H_1(q)$, are harmonic and expand the excited state about the equilibrium position of the ground state. In the second quantized form the vibrational Hamiltonians are

$$H_0 = \sum_i \hbar\omega_i(a_i^+ a_i + \tfrac{1}{2}) \tag{2}$$

$$H_1 = H_0 + \sum_i \{g_i(a_i + a_i^+) + V_i(a_i + a_i^+)^2\} + \hbar\omega_0, \tag{3a}$$

where g_i and V_i are the linear and quadratic coupling parameters for mode i. Note, these have units of energy. $\hbar\omega_0$ is the zeroth order energy gap between the ground and excited state surfaces. g_i and V_i are readily calculated from hole-burning data (Gillie et al., 1989) by Eq. 3, b and c:

$$g_i = S_i^{1/2} * \omega_i\hbar \tag{3b}$$

$$V_i = \frac{(\omega_i^e)^2 - (\omega_i^g)^2}{2 \cdot \omega_i^g}\,\hbar, \tag{3c}$$

where S_i is the Huang-Rhys factor for mode i. Superscripts "e" and "g" represent ground and excited states.

The optical absorption spectrum is given by

$$I(\omega) = \frac{1}{2\pi}\int_{-\infty}^{+\infty} dt e^{-i\omega t}\langle\langle \mu(t)\cdot\mu(0)\rangle\rangle e^{-\Gamma t}e^{-\gamma t^2}, \tag{4}$$

where $\mu(0) = \mu_{01}[|0\rangle\langle 1| + |1\rangle\langle 0|]$ and $\mu(t) = e^{iHt}\mu(0)e^{-iHt}$. Tracing over the electronic degrees of freedom and assuming that the transition dipole matrix element, μ_{01}, does not depend on the nuclear coordinates give

$$I(\omega) = \frac{\mu_{01}^2}{2\pi}\int_{-\infty}^{+\infty} dt e^{-i\omega t}\langle e^{iH_1 t}e^{-iH_0 t}\rangle e^{-\Gamma t}e^{-\gamma t^2}, \tag{5}$$

where

$$\langle e^{iH_1 t}e^{-iH_0 t}\rangle = \frac{Tr\rho_g(e^{iH_1 t}e^{-iH_0 t})}{Tr\rho_g}$$

represents a thermal average over the ground state density matrix (ρ_g) (Tr represents the trace operator). The parameter Γ gives a width to each vibronic transition above and beyond the intrinsic width that comes from low frequency modes contained explicitly in the Hamiltonian (i.e., spectral congestion). In what follows we take Γ to be the inverse of the sum of the radiative and nonradiative lifetimes (i.e., $\Gamma = 1/T_1$). T_1 is taken to be 3 ns for free Chl *a*. The only contribution to dephasing in this picture arises from the electron–phonon coupling to the 22-cm^{-1} phonon mode. Of course what is left out of this picture is the very large number of protein motions that are only weakly coupled to the optical transition. Thus, we underestimate the pure dephasing rate so our calculated spectral lineshapes should be seen as a lower limit for the homogeneous linewidth for a single site. The Hamiltonian is identical in form to that used by Hsu and Skinner in their theoretical studies of optical dephasing of impurity transitions in molecular crystals (Hsu and Skinner, 1984) and is similar to that discussed by Harris et al. as a simple model for pure dephasing in optical absorption (Harris et al., 1986). Inhomogeneous (Gaussian) broadening is introduced by the parameter γ, which corresponds to a Gaussian spectral width (200 cm^{-1}, FWHM (Hayes et al., 1988) of

$$\sigma = 4(\gamma \ln 2)^{1/2}. \tag{6}$$

To calculate the absorption spectrum we use the exponent combining algorithm developed by Friesner et al.

(1985). The interested reader is referred to this reference for details. We briefly sketch the matrix method here. The transition dipole autocorrelation function involves the thermal average of a product of exponentiated operators. The Hamiltonians of Eqs. 2 and 3a do not commute, and, moreover, the commutator of the two does not commute with either one, so the product of the two exponentiated forms is given by (Wilcox, 1967)

$$e^{iH_1t}e^{-iH_0t} = e^{i(H_1-H_0)t-1/2[H_1,H_0]t^2-i[H_1,[H_1,H_0]]t^3+\cdots}. \quad (7)$$

If the two Hamiltonians are quadratic in form, then the infinite series above can be summed in closed form and expressed in terms of an effective Hamiltonian operator $\tilde{H}$ (Balian and Brezan, 1969)

$$\langle e^{iH_1t}e^{-iH_0t}\rangle = \langle e^{i\tilde{H}t}\rangle. \quad (8)$$

After transforming to a suitable basis, the thermal average of this exponentiated effective Hamiltonian can be carried out exactly by using standard many-body techniques (Munn and Silbey, 1978). The exact nature of this method of exponent combining for harmonic degrees of freedom results from the fact that the boson creation and annihilation operators form a closed Lie algebra up to quadratic terms. The efficiency of this method allows routine calculation of absorption and emission spectra for large multimode systems.

Calculation of fluorescence spectra proceeds in exactly the same manner, however, the roles of H_0 and H_1 are reversed. This requires expanding the ground state Hamiltonian about the equilibrium position of the excited state and averaging over the excited state Hamiltonian. This results in a redefinition of the linear and quadratic coupling parameters. The fact that there are only minor quadratic interactions in few modes results in emission spectra that are essentially mirror images of the absorption spectra at the same temperature. In our simulations we take the emission lineshape of an individual species to be the mirror image of the absorption spectrum at that temperature. The emission maximum is determined by a Stokes shift of 7 nm (North et al., 1978) which is assumed to be temperature independent.

(b) Temperature dependence of PSI absorption spectral width

The Q_y region of the absorption spectrum of PSI is very broad ($\sim$660 cm^{-1}). The simulated absorption spectrum for the entire antenna complex can be obtained by introducing the contribution from static broadening or diagonal disorder. It has been proposed that there are multiple-spectral types of Chl *a* molecules in PSI (Ikegami, 1983; Ikegami and Itoh, 1988; Owens et al., 1988). Thus, the static broadening can be modeled by using several discrete spectral types of Chl *a* rather than a completely continuous distribution. The absorption lineshape of an individual spectral type is calculated according to Eq. 5. The inhomogeneous broadening (site broadening of each spectral type) in Eq. 5 is taken as 200 cm^{-1} (FWHM) from low temperature hole-burning experiments (Hayes et al., 1988). Justification for treating the inhomogeneous broadening in this manner comes from the fact that Chl *a* molecules in PSI are in a rigid protein environment. This site broadening only accounts for the continuous inhomogeneous broadening of the absorption lineshape of Chl *a* molecules in the PSI system. The spectral displacements between any two spectral types and the number of Chl *a* molecules in each spectral type are not temperature dependent, assuming that the structures of the proteins in PSI do not change significantly with temperature. The absorption spectrum of PSI is the result of a superposition of the spectrum of each spectral type. This approach is consistent with our treatment of the energy transfer dynamics.

In the weak coupling picture the broad absorption band of the antenna complex arises almost entirely from the types of broadening we have discussed. Exciton splittings between the Q_x and Q_y states of the Chl *a* in the protein are negligible compared with the linewidths of the individual sites. Under these circumstances the long range transport of energy occurs through a hopping mechanism with the individual single-step transfer rates given by Forster (1965). For excitation transfer between any two spectral types, we need to compute the spectral overlap between the relevant absorption (a) and emission (e) spectra for the two Chls. This is given by

$$F_{i\to j} = \frac{4\pi^2(10^{-24})\kappa^2}{h^2cn^4R_{ij}}\int_0^\infty \mu_a^i(\omega)\cdot\mu_e^i(\omega)\mathrm{d}\omega, \quad (9)$$

where R_{ij} is the distance between chromophores, κ the orientation factor, n the refractive index. μ_a^i and μ_e^i are the transition dipole moments for absorption and emission, respectively. The details of our method for computing the Forster rates will be given in the next section. We point out here that our use of the calculated spectra for the Chl *a* molecule coupled to the low frequency mode of the protein in the Forster calculation assumes that the protein motion is local in nature, i.e., that its correlation length is smaller than the inter-chromophore separation. The fluctuations in chromophore energies experienced at the donor site are thus completely uncorrelated from those at the acceptor site and the Forster picture is valid. Excitation transfer between chromophores coupled by a delocalized phonon has been discussed by other authors (Gillie et al., 1989; Lyle and Struve, 1991). Furthermore, the assumption of diagonal disorder within a given spectral type is problematic for the Forster calculation. In particular, no assumption is made concerning the correlation between spatial location and spectral position within a given spectral type. In the lattice models discussed in the next section, for the coarse grained inhomogeneous broadening (i.e., that due to the presence of different spectral types), the spectral–spatial correlation is, of course, treated explicitly. This results in two levels of averaging with regard to spectral disorder.

SIMULATION OF ENERGY TRANSFER

(a) Lattice model

Our approach to modeling energy transfer in PSI is based on a Forster hopping model (Pearlstein, 1982). The Forster transfer rate is determined by the overlap of the donor emission spectrum and the acceptor absorption spectrum. Direct integration of the product of the calculated absorption and fluorescence lineshapes yields the Forster overlap.

Alternatively, we fit the calculated single site absorption and fluorescence lineshapes with a Gaussian. $\mu^2(\omega)$ in Eq. 9 can be expressed as (Jean et al., 1988)

$$\mu^2(\omega) = \mu^2(\omega_0) \exp[-(\omega - \omega_0)^2/2\sigma^2], \qquad (10)$$

where the ω_0 denotes the peak frequency and σ the width of the band. $\mu^2(\omega_0)$ is chosen so that

$$\int_0^\infty \mu^2(\omega_0) \exp[-(\omega - \omega_0)^2/2\sigma^2]d\omega = \mu^2, \qquad (11)$$

i.e., the single site absorption and fluorescence lineshapes are normalized to their transition dipole strength, μ^2, which can be obtained from experiments (Shipman, 1977). The Forster rate constant F_{ij} in units of ps^{-1} for two sites thus can be calculated from the Gaussian lineshapes according to a formula derived by Jean et al. (1989):

$$F_{ij} = \frac{4\pi(10^{-24})\kappa^2}{ch^2n^4R_{ij}^6} \frac{\mu_i^2\mu_j^2}{\sqrt{2\pi\sigma_i\sigma_j}} \left(\frac{1}{2\sigma_i^2} + \frac{1}{2\sigma_j^2}\right) \times \exp\left[\frac{-\Delta_{ij}^2}{4\sigma_i^2\sigma_j^2}\left(\frac{1}{2\sigma_i^2} + \frac{1}{2\sigma_j^2}\right)^{-1}\right],$$

where Δ is the separation of donor emission and acceptor absorbance maxima.

At low temperature, the overall trapping time is limited by the energy transfer from low energy pigments (red pigments) to the reaction center (vide infra). The high frequency tail of the absorption spectrum and the low frequency tail of the fluorescence spectrum make little contribution to the energy transfer from 298–77 K. Thus, the Gaussian spectrum approximation appears justifiable for this study.

The number of spectral types and absorption maxima of the spectral types are chosen to be similar to those obtained by Ikegami and Itoh (1988). The absorption spectrum of PSI is obtained by summing the contribution of all individual spectral types weighted by the number of Chl of each spectral type. The number of Chl of each spectral type is determined by comparing the width of the calculated PSI absorption spectrum with the experimental value. In a few cases, the absorption maxima and the number of Chls of each spectral type used for simulations are obtained from deconvolution of the room temperature PSI absorption spectrum (for details, see next section).

We assume as an approximation that the structures of the proteins in the antenna system do not change with temperature. With this assumption, κ and R_{ij} will have no temperature dependence. We also assume that the refractive index and transition dipole strengths have no temperature dependence. As described in the previous section, the spectral width of individual spectral types will be temperature dependent. The fluorescence spectral width of an individual spectral type is assumed to have the same value as the individual absorption spectral width because of the absence of significant frequency shifts between S_0 and S_1.

A change of temperature not only has an effect on the Forster rate but also on the trapping kinetics in the Master equation as shown below (Jean et al., 1989),

$$dp_i(t)/dt = \sum_j F_{ij}p_j(t) - \sum_j F_{ji}p_i(t) - \tau_i^{-1}p_i(t), \qquad (13)$$

where $p_i(t)$ is the probability that an excitation resides on the ith site at time t; F_{ij} is the rate constant for energy transfer from pigment j to pigment i, and $1/\tau_i$ is the rate for all decay processes other than energy transfer (τ_i is 3 ns for fluorescence of free Chl). When i corresponds to the reaction center, $1/\tau_i$ is the rate constant for charge separation plus the $(3\ ns)^{-1}$ radiative rate constant. The reverse rate (or uphill transfer rate) is calculated from the downhill rate using the detailed balance condition,

$$F_{ij} = F_{ji} \exp(-\delta A_{ij}/kT), \qquad (14)$$

where δA_{ij} is the difference between the peak frequencies of the two absorption bands. This assures that in the absence of deexcitation, the site populations relax to a Boltzmann distribution. Thus, the ratio of the uphill and downhill rates for any pair of pigments is strongly temperature dependent. The charge separation rate may also be temperature dependent. We assume that the temperature dependence of the charge separation rate is small in the temperature range 77–298 K. This is justified from the experimental results of the temperature dependence of bacterial RC (Fleming et al., 1988). We also assume that the number of Chl per spectral type and the absorption maxima of individual spectral types are not temperature dependent because they are determined by the protein perturbations.

TABLE 1 a Peak wavelengths of absorption and fluorescence of all spectral types

Spectral type	λ_{max}	
	Absorption	Emission
	nm	
A	700	707
B	697	704
C	705	712
D	692	699
E	687	694
F	682	689
G	677	684
H	669	676

(b) Model systems

Although the numerical calculation method (Jean et al., 1989) provides us with a powerful tool to simulate energy transfer with different models, many issues have to be addressed. For example, do the PSI particles contain pigments that absorb at a wavelength longer than the RC (P700)? Presupposing their existence, how are these red pigments and other spectral types arranged? Are the red pigments close to the RC so that they are directly coupled to the RC? Why is there so little temperature dependence of the overall trapping time in PSI (Werst et al., 1992)? One expects that a deep alternative trap will give a strong increase in the fluorescence lifetime at low temperatures. What is the origin of the fluorescence emission wavelength dependence of the decay time at low temperature? This latter question is of particular interest in the red region of the spectrum ($\lambda_{em} \geq 700$ nm). Without one or more red pigments, the experimentally observed red emission would be unlikely. Is there any rate-limiting process in PSI at low temperatures? From the expression for the uphill transfer rate (Eq. 14), one can predict that slow uphill transfers from red pigments should limit the overall trapping time at low temperature if the charge separation rate is not strongly temperature dependent. Do two or more different uphill transfer rates result in wavelength dependence of fluorescence emission lifetime? The different uphill transfer rates can occur when particular spectral types have different neighbors. Is a random distribution of spectral types in the PSI core antenna adequate to describe the observed wavelength dependence? All these issues play critical roles in modeling energy transfer in PSI. A successful model should have the ability to explain both the wavelength and temperature dependence observed experimentally.

TABLE 1 *b* **Number of Chl *a* of every spectral type for the lattice models 1–9**

Spectral type	Models								
	1	2	3	4	5	6	7	8	9
A	1	1	1	1	1	1	1	1	1
B	0	2	0	2	2	2	0	0	2
C	0	2	0	2	2	2	4	4	2
D	4	4	4	4	4	4	4	4	4
E	8	7	8	7	7	7	6	6	7
F	9	8	9	8	8	8	8	8	8
G	13	12	13	12	12	12	12	12	12
H	14	13	14	13	13	13	14	14	13

The model systems we simulated contain 49 pigments (sites) comprising 48 core antenna and one reaction center (700 nm). The number of sites is chosen to mimic the core antenna size of the PSI particles studied by Werst et al. (1992). A total of nine models were studied. In these models, the number of pigments for each spectral type and their absorption maxima (see Table 1) were chosen to yield an absorption width at 298 K that approximates the absorption width obtained from experiments. Increasing or decreasing the number of spectral types by 1 (705 and 700 nm spectral types are not included) does not alter the simulation results. Particularly, simulations with or without a 697-nm band do not change our conclusions. The use of a 697-nm band and the choice of the absorption maxima of P700 (700 nm) and the red pigments (705 nm) are made in order to test models proposed by Wittmershaus (1987) and by Mukerji and Sauer (1989). The calculated absorption spectral width at 77 K is also close to the experimental result. Using fewer spectral types, the calculated absorption spectrum at 77 K tends to show an unreasonably structured spectrum. It should be pointed out that there is no unique way to assign the number of pigments for each spectral type since we do not know the exact number of spectral types in PSI and the exact position of the absorption maximum of the individual types. Varying the number of Chl *a* per spectral type (apart from the red pigments) within ±3 does not alter our conclusions. Whenever the selection of the number of red pigments makes a difference to our simulation results, we state the results separately. Simulation results also show that shifts of ±3 nm in the absorption maxima of individual spectral types (including P700 and the red pigments) do not influence our conclusions. Unless otherwise stated, the spectral properties used in the dynamical calculations are those of Table 1. To study the two most promising models (the random model with 1 red pigment and the random model with red pigment(s) fixed close to the RC) in detail, we also repeat simulations that used the spectral types obtained by deconvoluting the room temperature absorption spectrum of the PSI particles. During the deconvolution, the position of P700 is constrained to lie in the wavelength range 694–700 nm. The position of the red pigments is also fixed to a wavelength between 702–705 nm. The number of Chls per spectral type was determined directly from the amplitude of each Gaussian component. Individual spectral components obtained from this procedure are shown in Fig. 1. The simulation results according to the spectral properties in Table 1 or Fig. 1 show little difference. In all the simulations, the width of every spectral type is taken to be the same and is obtained from the results of absorption lineshape calculations at the given temperature. The center-to-center distance between sites in models 1–9 is 11.5 Å. This is consistent with estimates based on the pigment and protein densities and with the experimentally observed Chl–Chl distance in LHCII (Kuhlbrandt and Wang, 1991). A time constant of ~1 ps for pairwise transfer to a neighboring site at 298 K is obtained at this distance. This is similar to that obtained experimentally by Owens et al. (1987). The charge separation time is 3.4 ps (Owens et al., 1987). Assuming the orientations of Chl *a* in PSI are random, the orientation factor, κ^2, is set to two-thirds as the result of a static average. The transition dipole strength μ^2 is chosen to be 21.7 D^2 (Shipman, 1977). Nonneighbor hopping between sites is included. This is expected to become more important at low temperatures because it facilitates the escape of an excitation from a low energy species (an alternative trap) in the antenna. The fluorescence decay time in the absence of energy transfer and trapping is taken as 3 ns for all sites. A time step of 5 ps was used for most of the calculations. The excitation wavelength is chosen as 654 nm to simulate the conditions used in the single photon counting measurements (Werst et al., 1992). The initial (t = 0 ps) population of a spectral type is calculated according to the contribution to the absorption cross-section of the given spectral type at the excitation wavelength (Jean et al., 1989). The initial excitation density of a spectral type is then evenly distributed among sites of the same spectral type.

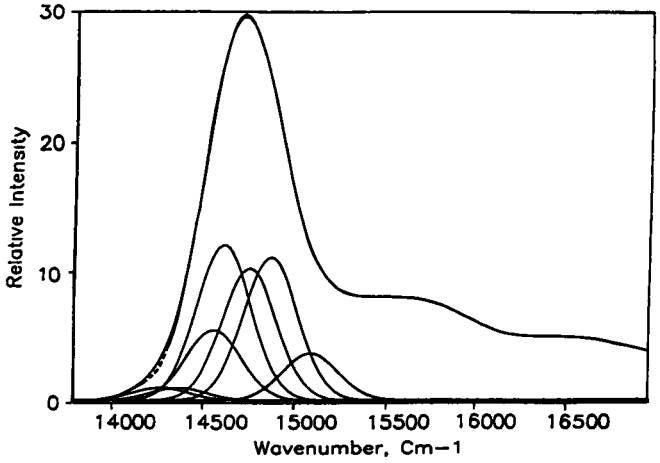

FIGURE 1 Absorption spectra of the PSI particles. The broken line (– – –) represents the experimentally obtained absorption spectrum of the PSI-40 core particle; the solid line (——) represents the simulated absorption spectrum and individual gaussian components. The fit extends across the full range of the plot, including the Q_y (0–1) and Q_x transitions. The peak positions and relative amplitudes of the Gaussian components are: 703 nm, 1; 697 nm, 1 (P700); 686 nm, 6; 683 nm, 13; 675 nm, 11; 669 nm, 12; 657 nm, 5. The Q_y (0–1) and the Q_x transitions are both represented by two Gaussian components.

We first outline our studies and in the following paragraphs give detailed descriptions of each of the models. We begin our simulations with funnel and random models without and with red pigments. Models 1–4 (Fig. 2) simulate four extreme cases: the funnel model, the

Model 1 (Funnel)	Model 2 (Funnel)	Model 3 (Random)	Model 4 (Random)
H H G F G H H	H H H H H H H	G E G G H G E	H F H G H E H
H G F E F G H	H E E E E E G	F H D E E E F	H H C G D D G
G F E D E F G	H E D C D F G	H H G H E F H	G F B H E G H
G E D A D E G	H E C A B F G	H E D A F D H	H G C A G E G
H F E D E F H	H E D B D F G	H F F H G F F	F F G H H E G
H G F E F G H	H F F F F G G	F H G G G G D	E F E E D G G
H H G G G H H	H G G G G G G	G H E G G H H	F F H D F H B

FIGURE 2 Model lattices with multi-spectral types used to simulate the organization of the PSI core antenna. Model 1 is a funnel model without red pigments. Model 2 is a funnel model with red pigments (*C*) next to the reaction center (*A*). Model 3 is one representative configuration (out of 50 configurations used for the simulation) of a random model without red pigments. Model 4 is one representative configuration (out of 50 configurations used for the simulation) of a random model with two red pigments. The code for the various spectral forms (letters *A–H*) is given in Table 1 *a*.

Model 5	Model 6	Model 7	Model 8
G G F F F G G	B H G G G H B	C H G H G H C	C H G H G H C
G F F F F F G	H H F E F H H	H H F G F H H	H H F G F H H
G E E E E E G	G F E D E F G	G F E D E F G	G F E D E F G
G E D A D E G	G E D A D E G	G E D A D E G	G E D A D E G
G H D B D H G	G F E D E F G	G F E D E F G	G F E D E F G
H H H B H H H	H H F G F H H	H H F G F H H	H C F G F H H
H H C C H H H	C H G H G H C	C H G H G H C	H H G H G H C

FIGURE 3 Model lattices for the study of temperature and wavelength dependence of energy transfer in the PSI core antenna. Model 5: Two 705 nm red pigments (*C*) are coupled to the reaction center (700 nm; *A*) through two 697-nm bridging pigments (*B*); model 6: two kinds of pseudo-traps (*B* and *C*) are located away from the reaction center (*A*); model 7: only one kind of pseudo-trap (*C*) is present and located away from the reaction center (*A*); model 8: only one kind of pseudo-trap (*C*) is present but pseudo-traps are not in the same environments. The full code for the spectral forms is given in Table 1 *b*.

funnel model with additional red pigments close to the reaction center, and random models without or with red pigments. Use of the word random here is not meant to convey disorder in the relative positions of pigments, rather the absence of a correlation between spectral type and spatial position. Model 1 (Fig. 2) is a funnel model in which the core antenna types are arranged so that as one moves out radially from the trap, the absorption spectrum of the individual pigments shift progressively to shorter wavelengths. No red pigments are included. All the pigments that belong to the same spectral type have similar neighboring pigments (i.e., have similar environment). Model 2 (Fig. 2) is also a funnel type model but two additional low energy spectral types (B, 697 nm; and C, 705 nm) each with two pigments are included. These four additional pigments are arranged close to the trap so that the red pigments can channel energy toward the RC (Wittmershaus, 1987; van Grondelle, 1988). The rest of the pigments are arranged so as to provide two different energy channeling paths to the RC. The two 697 and 705 nm pigments have identical environments. Model 3 (Fig. 2) is a random model without red pigments in which pigments of different spectral types are haphazardly arranged around the trap. A random model (model 4) with these additional "red" spectral types was also studied (Fig. 2). In both of the funnel-type models (Fig. 2, model 1 and model 2), the spatial arrangements of all pigments are ordered so that the energy transfer is most efficient. We shall show that these funnel and random models are not adequate to describe the experimental data.

Models 5–8 (Fig. 3) are used to address the issues raised above and to understand the temperature and wavelength dependence of the fluorescence decay obtained in models 1–4. From these calculations we propose model 9 (Fig. 4) to simulate the experimentally observed temperature and wavelength dependence of PSI particles and to compare with model 4. In model 5 (Fig. 3), the two red pigments (705 nm) are away from the reaction center and the two 697 nm pigments serve as a bridge for facilitating the escape of excitation from the additional traps (i.e., the red pigments) in this model. The other pigments that surround the red pigments are significantly bluer so that at low temperature the uphill transfer from red pigments to reaction center occurs only through the 697-nm pigments neighboring the red pigments at low temperature. The two red pigments (705 nm) have effectively similar environments because an excitation, after concentrating at a red pigment, has to escape through the same 697-nm pigments. Therefore, the wavelength dependence of the trapping dynamics is expected to be small in model 5. However, the temperature dependence is expected to be larger in model 5 than in model 2. In model 6 (Fig. 3), the two 705 and two 697 nm pigments are at the corners of the array. This arrangement is intended to focus energy to two different kinds of pigments, i.e., the 697 nm pigments and 705 nm pigments which are distant from the reaction center. The arrangement is intended to probe the effect of the two different kinds of alternative traps on the overall trapping dynamics, in particular the wavelength dependence. In model 7 (Fig. 3), we try to confirm the wavelength dependence of the trapping kinetics we obtained in model 6 by substituting the two 697-nm pigments with another two 705 nm pigments. In model 8 (Fig. 3), one red pigment is in a different environment from the other three red pigments. In model 9 (Fig. 4), the two red pigments are placed next to the reaction center, whereas other pigments are randomly arranged. For the random models, i.e., models 3, 4 and 9, the reported decays from 50 configurations of the arrangements of spectral types are averaged for each calculation of a random model.

RESULTS AND DISCUSSION

(a) Chl *a* and PSI absorption spectra

The temperature dependence of the calculated absorption lineshape of a single spectral type of Chl *a* bound to a protein, represented by a single low frequency mode of 22 cm^{-1} (Gillie et al., 1989) is shown in Fig. 5. An inhomogeneous width of 200 cm^{-1} (Hayes et al., 1988) has been added to bring the calculated width into closer agreement with experimental results (Fig. 1). The total linewidth (FWHM) of the main peak narrows from 430 cm^{-1} at 298 K to 235 cm^{-1} at 30 K. As expected, the homogeneous contribution to the width, due largely to the low frequency protein phonon, decreases sharply with temperature. There is also a very slight red shift, ~2 nm, that occurs on lowering the temperature. The use of an Einstein model for the protein is certainly unrealistic, however, the dominance of the 22-cm^{-1} mode in the hole-burned spectra of Gillie et al. (1989) suggests that this simple model will provide the correct qualitative trend in the reduction of the lineshape, and therefore the effect of this lineshape on the Förster overlap, at low temperature. The chlorophyll vibrational frequencies, linear and quadratic coupling constants used in the spectral calculations are shown in Table 2.

Knowledge of the lineshapes of the individual spectral types of Chl *a* allows us to determine the absorption maxima of each spectral type as well as the number of pigments of each type by comparison with the experimental absorption spectrum obtained from the PSI. Results obtained by fitting the number of spectral types,

Model 9 (Random)
H F E B H H F
D E G E G H H
F G E D F H B
F D C A G G G
H E H C G F H
F D H E H G G
E G F H H G G

FIGURE 4 Model 9, one representative configuration (out of 50 configurations for the simulation) of the random model with two red pigments (*C*) located next to the reaction center (*A*). The code for the spectral forms is given in Table 1 *a*.

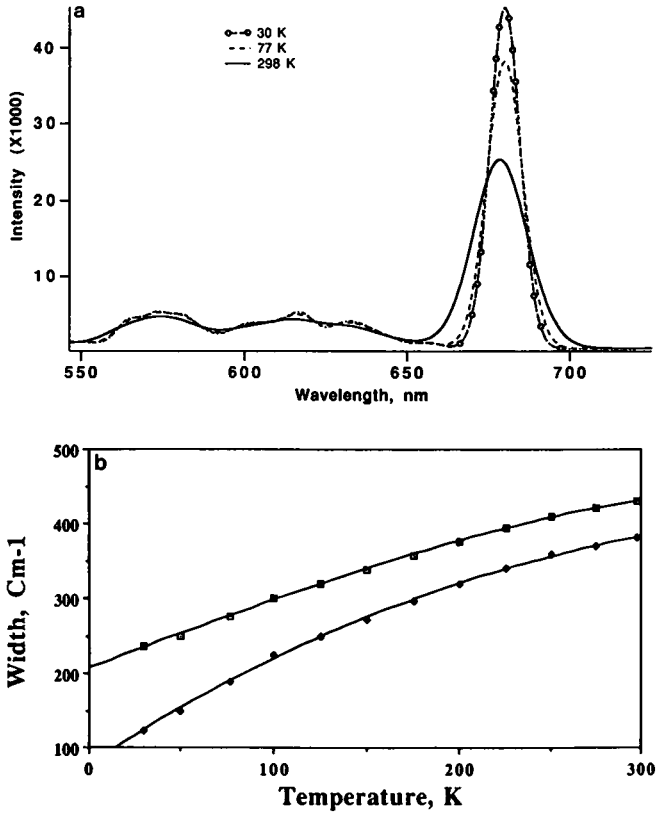

FIGURE 5 (*a*) Temperature dependence of the calculated absorption lineshape of a single spectral type of Chl *a* bound to a protein. The solid line (——), the dashed line (------), and the beaded line (—○—) represent the calculated curves at 298, 77, and 30 K, respectively. The calculated spectral widths (including 200 cm^{-1} site-broadening width) in cm^{-1} are 430 (298 K), 420 (275 K), 410 (250 K), 394 (225 K), 376 (200 K), 357 (175 K), 338 (150 K), 319 (125 K), 300 (100 K), 275 (77 K), 250 (50 K), and 235 (30 K). (*b*) Absorption spectral widths at different temperatures. The line with open squares (—□—) represents the total Q_y absorption band width (FWHM) of an individual spectral type from 30–298 K. The line with filled squares (—■—) represents the homogeneous Q_y absorption band width (FWHM) for the individual spectral type.

their amplitudes, and peak positions are shown along with the experimental result for PSI particles at 298 K (Fig. 1). The number of spectral types and the absorption maxima of each spectral type are similar to those obtained by Ikegami and Itoh (1988). Inclusion of pigments redder than P700 is consistent with Ikegami (1983), who found red pigments (700–702 nm) in reconstituted PSI particles containing 29 Chl *a* molecules per P700.

(b) Simulations in PSI

Simulation of PSI particles

In the first set of simulations, models 1–4, we focus on two issues: (*i*) whether funnel or random models are capable of reproducing the experimental trends in the temperature and wavelength dependent fluorescence decays, and (*ii*) whether low energy species ("red pigments") are required in these models.

Simulations of energy transfer in the funnel model without red pigments (model 1, Fig. 2) show single exponential kinetics. The lifetime of the excitations in this model decreases from 24 ps at 298 K to 3.5 ps at 77 K and is independent of emission wavelength. This result is expected because at low temperature (77 K) the excitation is concentrated on the RC in less than a few picoseconds and the energy transfer from the RC back to the core antenna (uphill transfer) is slow because of the Boltzmann factor. Thus, the overall trapping time is lim-

TABLE 2 **Parameters for absorption lineshape calculations (cm^{-1}): PSI S_1 and S_0 vibrational frequencies, Huang-Rhys factors, linear displacements, and frequency shifts**

S_1 Vibrational frequency*	S Huang-Rhys factor*	S_0 Vibrational frequency‡	g_i Linear displacements	V_i Frequency shift
22	0.800		19.7	
262	0.012	260	28.7	2.0
283	0.004		17.9	
390	0.015	390	47.8	0.0
425	0.007		35.6	
469	0.019	470	64.6	−1.0
501	0.007		41.9	
521	0.017	520	67.9	1.0
541	0.009		51.3	
574	0.025	570	90.8	4.0
588	0.005		41.6	
607	0.012		66.5	
638	0.009		60.5	
692	0.015		84.8	
714	0.010		71.4	
746	0.044	745	156.5	1.0
771	0.007		64.5	
791	0.014		93.6	
805	0.012		88.2	
819	0.005		57.9	
855	0.009		81.1	
864	0.007		72.3	
874	0.007		73.1	
896	0.013		102.2	
932	0.025	915	147.4	17.2
994	0.028		166.3	
1009	0.005		71.3	
1075	0.012		117.8	
1114	0.009		105.7	
1178	0.018	1185	158.0	−7.0
1203	0.012		131.8	
1259	0.041		254.9	
1285	0.011		134.8	
1340	0.011	1385	140.5	−44.3
1364	0.032		244.0	
1390	0.018		186.5	
1411	0.005	1430	99.8	−18.9
1433	0.009		135.9	
1455	0.006		112.7	
1465	0.006		113.5	
1504	0.010	1525	150.4	−20.9
1524	0.032	1545	272.6	−20.9

* From Gillie et al. (1989). ‡From Avarmaa and Rebane (1982).

ited by the charge separation rate. These simulations suggest that the relatively small temperature effects observed experimentally (Werst et al., 1991) are not consistent with a funnel description of antenna organization and energy transfer allowing us to exclude this model from further consideration. It was shown previously (Jean et al., 1989) that the ability to detect short components using the single photon counting method can be compromised by the presence of long lifetime components. In this work, we will show that the short component of a decay curve obtained from fitting can be significantly altered if the original decay curve is highly nonexponential. However, it should be pointed out that the time constant for the largest amplitude component is insensitive to the addition of noise and long lifetime components, or to convolution with an instrument function, if the original decay curve can be fitted to one or two components. When the decay is single exponential, these effects are negligible and thus only decay curves calculated from the random models at 77 K need to be convoluted with an instrument function to obtain time constants appropriate for comparison with experimental results.

Simulations using the funnel model with red pigments close to the trap (model 2, Fig. 2) show very weak temperature dependence, with τ = 35 ps at 298 K and 41 ps at 77 K. The small temperature dependence can be explained by the balance of the rapid concentration of excitations on the red pigments and the slow uphill transfer from the red pigments to the reaction center. The red pigments are the major source of emission at 77 K. There is no emission wavelength dependence in this model because the slow uphill transfer from the red pigments to the reaction center determines the wavelength dependence and the two red pigments have similar environments. More detailed studies of the wavelength dependence will be discussed for models 5–8. The lack of spectral dependence of the trapping time in model 2 enables us to exclude it. The simulation results at 30 K show a significant decrease of the energy trapping rate (560 ps decay time). Our results are unlikely to be realistic at very low temperature because we ignore the temperature dependence of the charge separation rate. In addition, the actual three-dimensional arrangement of pigments should be included at low temperatures. In three-dimensional models, more pigments are close to the RC than in two-dimensional models. The energy transfer in three-dimensional models will be more efficient at low temperature because an excitation on a given pigment has a larger number of possible low energy pathways to the RC. At high temperature, the difference in trapping times between two- and three-dimensional models containing the same number of pigments is small because the uphill transfer rate is fast.

The lifetime of the excitations for the random model (model 3, Fig. 2) without red pigments at room temperature is ~36 ps and emission wavelength independent (see Table 3). The decays at low temperature are nonexponential and show that the lifetime increases between 680 and 700 nm and decreases between 700 and 720 nm at 77 K. To compare with experiments, we added two low amplitude long lifetime components (800 ps and 4 ns) and convoluted the simulated curve with a measured instrument response function. An example of the decay after convolution is shown in Fig. 6. On fitting the resulting curve and extracting the short component we find that at 77 K, the lifetime increases from 14.5 to 21 ps as the emission wavelength is increased from 680 to 700 nm. This increase reflects the presence of shallow traps, i.e., redder antenna pigments surrounded by bluer pigments. Since the difference among all the antenna spectral types is small in this model, the pseudo-traps are not deep. The phonon energy required for the excitation to leave the shallow trap is comparable to k_bT at 77 K, so the calculated wavelength dependence is small. The lifetime decreases from 21 to 14 ps for emission wavelength from 700 to 720 nm. This is because P700 is the spectral type with the lowest energy in model 3. The redder the emission wavelength we monitor, the greater the contribution from the reaction center. The emission from the reaction center is efficiently quenched by the rapid charge separation process, so the apparent decay time constant decreases from 700 to 720 nm. These wavelength-dependent results are not consistent with experiments.

The lifetime of the excitation at 298 K for the random model, which includes red pigments, (model 4, Fig. 2) is ~50 ps and shows minor wavelength dependence (see Table 4). At 77 K the decay kinetics are multi-exponential and strongly wavelength dependent. This wavelength dependence is clearly seen in the average fluorescence lifetime which is defined as

$$\tau_{avg} = \sum A_i \tau_i,$$

where τ_i (time constant for the ith component of the decay) and A_i (corresponding amplitude) are obtained directly from the simulated curve. τ_{avg} is correlated with the trapping kinetics. To compare with experiments, we added two low amplitude long lifetime components and convoluted the simulated curve with a measured instrument response function. The fluorescence lifetimes change significantly when one or two red pigments are included in the random model. If two red pigments are included, the fits (Table 4) show that the amplitude of the fast component is strongly wavelength dependent at 77 K in contrast with the experimental data of Werst et al. (1992). A slow rise time also shows up clearly in the long wavelength emission, which is due to the lack of the funnel process, because excitation cannot directly visit the red pigments without being trapped by other shallow pseudo-traps. A corresponding decay component in the blue part of the spectrum is not observed because of the large number of overlapping rise and decay components

TABLE 3 **Time constants obtained from the fitting results of simulations using model 3**

Temperature	Emission	Decay parameters							
		τ_1	A_1	τ_2	A_2	τ_3	A_3	τ^*	A^*
K	*nm*	*ps*		*ps*		*ps*		*ps*	
298	680	0.3	0.026	32.5	0.780	48.1	0.194	36.4	0.926
	690	0.1	0.003	32.6	0.799	48.0	0.198	36.5	0.927
	700	0.1	−0.005	31.8	0.730	45.7	0.275	36.6	0.928
	710	0.1	−0.010	32.9	0.842	48.8	0.168	36.4	0.928
	720	0.2	−0.017	32.4	0.829	47.3	0.188	36.0	0.928
77	680	5.7	0.588	29.3	0.343	117.2	0.069	14.5	0.698
	690	16.2	0.360	49.1	0.468	139.0	0.172	17.8	0.569
	700	17.5	0.302	53.2	0.506	142.5	0.192	20.6	0.433
	710	10.6	0.336	42.9	0.490	129.9	0.174	16.6	0.559
	720	8.1	0.450	33.3	0.450	111.5	0.100	13.8	0.726

The excitation wavelength is 654 nm. τ^* and A^* are the fast component and its amplitude obtained from the fit after two long lifetime components (800 ps, 7%; 4.4 ns, 4%) have been added to the decay. The decay is also convoluted with a 60-ps measured instrument function and Gaussian noise is also added. $\chi^2 \leq 1.2$.

in this region. The 705-nm pigments in this model constitute deep pseudo-traps at low temperatures. The environment of the two spectral types may be quite different.

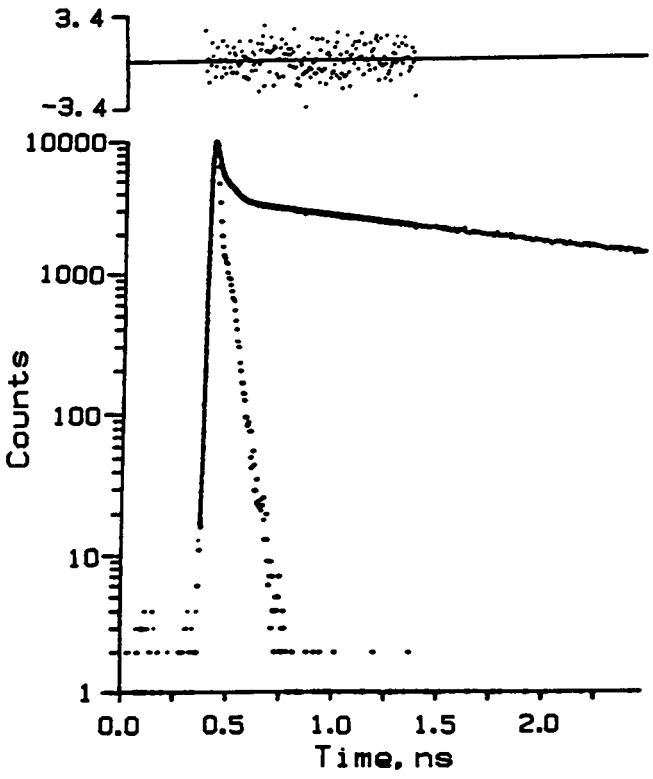

FIGURE 6 Fluorescence decay curve calculated for model 3 (random model with red pigments next to the reaction center). The lifetimes are listed in Table 3. Excitation and emission wavelengths are 654 and 680 nm, respectively. Two long lifetime components (800 ps, 7%; 4.4 ns, 4%) have been added to represent the antenna without traps and disconnected Chls according to Werst et al. (1991). The decay has been convoluted with a 60-ps measured instrument function. Gaussian noise was also added. $\chi^2 = 1.1$.

Some of the pseudo-traps and the reaction center may be coupled to each other by a "local funnel path" in an otherwise random model. All the above factors may cause the strong wavelength dependence and multi-exponential kinetics in the model. The only case in which an alternative trap will accelerate the energy transfer to P700 is when the red pigments are close to the RC. By directly coupling red pigments with the reaction center, less emission wavelength dependence is expected because the red pigments cannot form deep traps in this configuration. An alternative way to have a smaller emission wavelength dependence is to have fewer red pigments. If only one red pigment is included and the spectral properties are used according to deconvolution results from Fig. 1, the lifetimes (amplitudes) at 77 K, obtained after convolution with noise, instrumental function, and long lifetimes component are 13.4 ps (67.4%) at 680 nm, 15.2 ps (65.6%) at 690 nm, 20.4 ps (52.0%) at 700 nm, 97.2 ps (50.0%) at 710 nm, and 104 ps (48.6%) at 720 nm. This result is similar to the experimental data of Werst et al. (1992). So we cannot rule out the "completely" random model with one red pigment. The important conclusion here is that including one or more red pigments in the random array is necessary for the simulation of the observed wavelength dependence of fluorescence lifetimes. The relatively small change in lifetime for the temperature range 70–36 K (Werst et al., 1992) suggests that the red pigment(s) is close to the trap. A red pigment away from the trap would result in more drastic temperature dependence (see results from models 5–8).

In the following four simulations (models 5–8) motivated by suggestions of Wiltmershaus (1987) and Mukerji and Sauer (1988) on the location of the red pigments, we examine how the pigment location influences the time and wavelength resolved decays.

The decay of the excitation in model 5 (Fig. 3) for which the red pigments are not close to the reaction

TABLE 4 **Time constants obtained from the fitting results of simulations using model 4**

Temperature	Emission	Decay parameters										
		τ_1	A_1	τ_2	A_2	τ_3	A_3	τ_4	A_4	τ^*	A^*	τ_{ave}
K	*nm*	*ps*		*ps*		*ps*		*ps*		*ps*		*ps*
298	680	0.2	0.180	38.3	0.293	54.3	0.527			48.0	0.918	
	690	0.2	0.157	37.5	0.277	54.0	0.566			48.5	0.921	
	700	0.2	0.086	39.8	0.335	54.4	0.579			49.9	0.927	
	710	4.7	−0.137	47.2	0.947	62.3	0.190			51.4	0.936	
	720	6.8	−0.181	47.2	0.965	61.7	0.216			51.7	0.941	
77	680	0.2	0.430	7.4	0.443	32.4	0.115	177.4	0.012	9.2	0.836	9.31
	690	6.8	0.357	22.5	0.453	80.2	0.165	315.9	0.025	12.1	0.749	33.7
	700	10.5	0.406	58.1	0.419	302.8	0.175			17.2	0.478	79.5
	710	0.1	−0.060	99.9	0.611	496.3	0.449			11.1	−0.066	284
	720	7.1	−0.457	101.9	0.723	474.7	0.734			15.0	−0.335	419

The excitation wavelength is 654 nm. τ^* and A^* are the fast component and its amplitude obtained from the fit after two long lifetime components (800 ps, 7%; 4.4 ns, 4%) have been added to the decay. The decay is also convoluted with a 60-ps measured instrument function and Gaussian noise is also added. $\chi^2 \leq 1.2$.

center shows no wavelength dependence at 77 K. This is due to the fact that there are only two possible rate determining processes in the model, i.e., the two uphill transfers from the two red pigments toward the trap. The environments of these red pigments are similar as we pointed out previously, therefore, only one rate determining process exists in the model, which results in no wavelength dependence. The lifetime increases from 37.6 to 68.4 ps as the temperature decreases from 298 to 77 K at all emission wavelengths, although a low energy pathway between the 705-nm pigments and the RC (see model 5, Fig. 3) is provided by the 697-nm pigments. Destroying this pathway will cause a further increase in the lifetime when the temperature is decreased. This effect will be clearly seen in model 6. The temperature dependence in model 5 is not consistent with the experimental results in which the lifetime decreases from 295 to 77 K between 680 and 690 nm. The temperature dependence of model 5 can be understood by comparing this model with model 2 (Fig. 2) in which the red pigments are close to the trap. In model 2, the excitation will remain close to the RC after the excitation is concentrated on the 705-nm pigments. However, this is not the case in the model 5 in which the transfer out of the red pigments can lead the excitation back to the antenna more easily. For the model with the red pigments not close to the trap (model 5), the lifetime will show a large increase from high temperature to low temperature. It is clear that the red pigments must be close to the trap in order to obtain a small temperature dependence.

To show that the two different kinds of uphill steps (from C to A or from B to A) can yield a wavelength dependence in the fluorescence decay kinetics, we simulated trapping kinetics in model 6. The low energy pathway presented in model 5 is nonexistent and four deep traps are formed. The two 697-nm pigments and the two 705-nm pigments form traps with different depths and thus two different uphill transfer processes. A strong temperature dependence is expected because the red pigments are distant from and therefore decoupled from the trap. In fact, the energy transfer is so slow that the charge separation time (~3 ps) shows up separately from the overall trapping time (see Table 5). The red pigment(s) cannot be located away from the RC to show a small temperature dependence. The long overall trapping time for model 6 is strongly wavelength dependent in agreement with our prediction. From the simulations, we determine that the strong wavelength dependence of the fluorescence comes from the two significantly different kinds of pseudo-traps (B or C) formed in this model. One way to reduce the wavelength dependence is to couple the red pigments to the RC as we will show in model 9.

We simulated model 7 to show that one slow uphill transfer rate (i.e., all the rate determining pigments having the same environment) is not sufficient to generate a wavelength dependence at 77 K. In model 7, the 697-nm pigments are replaced by 705-nm pigments and all the red pigments are in the same environment. The other antenna pigments also have the same or similar environments. No wavelength dependence of the lifetimes (τ_1 = 3.4 ps and τ_2 = 1865 ps) is found. The reason for this is

TABLE 5 **Time constants obtained from the fitting results of simulations using model 6**

Temperature	Emission	Decay parameters			
		τ_1	A_1	τ_2	A_2
K	*nm*	*ps*		*ps*	
77	680	3.4	0.998	860	0.002
	690	3.4	0.983	540	0.017
	700	3.4	0.956	613	0.044
	710	3.4	0.934	1156	0.066
	720	3.4	0.555	2855	0.445

The excitation wavelength is 654 nm.

that at low temperature the excitation very quickly (~5 ps) becomes concentrated on the lowest energy spectral type. After this time, with only one kind of pseudo-trap, the emission is simply the spectrum of this species, i.e., the emission is time independent. With more than one kind of pseudo-trap, the spectrum will evolve as the relative excitation densities of the pseudo-traps change with time. This feature is an intrinsic property of the random models.

To understand the emission wavelength dependence in more detail, in particular the comparatively weak wavelength dependence observed in experiments, another model system was studied (model 8) in which three of the four red pigments have the same environment. We ignore the charge separation time and focus our attention on the long trapping times which are 409–450 ps at emission wavelengths from 680–720 nm at 77 K. Since the difference of the environments of the four 705-nm pigments is not large, this weak wavelength dependence is expected. To summarize the studies of the emission wavelength dependence, we conclude that at low temperatures a strong wavelength dependence of the fluorescence lifetime in a model array will occur if several different deep traps form. These deep traps could be formed by different types of pigments or by different pigments belonging to the same spectral type in different environments. Of course weak wavelength dependence may also arise from shallower traps.

We conclude that pigment(s) with energy lower than P700 must be close to the trap (in the first or the second shell around the trap) to produce an acceptable temperature dependence. The random distribution of the rest of the pigments generates both deep and shallow traps. Most importantly these traps have different environments and produce a low temperature emission wavelength dependence of the trapping time similar to the experimentally observed results. A simple way to describe the arrangement of these pigments is to use a random model for all except the red pigments. To test these ideas we constructed a final model in which the red pigment(s) are fixed close to the trap and other antenna pigments are randomly arranged (model 9). When two red pigments are included, at 298 K, this model gives a lifetime of 41 ps with little wavelength dependence (see Table 6). At 77 K we add two long lifetime components (800 ps, 4.4 ns) and convolute as described above. The short component after the convolution varies from 10 ps to 57 ps as the wavelength increases from 680 to 720 nm. Including one red pigment and using spectral properties according to Fig. 1, the lifetime of the short component after the convolution varies from 14 to 44 ps (680–720 nm). Thus, this model shows the same trends in the wavelength and temperature dependence as the experimental data.

Fig. 7 shows calculated time-resolved emission spectra for a random model with one red pigment fixed close to the RC at both 77 and 298 K with 654 nm excitation. The key issue determining the sensitivity of the fluorescence lifetime with emission wavelength is the time it takes the excitation to become spectrally random compared with the trapping time. This will of course depend both on the single step transfer time and on the local environment near the pigments that are excited, in other words the number of "hops" an excitation has to make before it visits a representative number of spectral types. In Fig. 7 *a* it is seen that the emission spectrum at 298 K undergoes spectral evolution over the first few picoseconds reaching a quasi-steady-state in less than 4 ps. At longer times there is a very slight narrowing of the low energy side of the lineshape resulting from transfer of excitations from red pigments to the nearby P700 and subsequent irreversible electron transfer. Thus, the fast spectral equilibration time results in trapping kinetics that are independent of emission wavelength. In Fig. 7 *b* the time-evolution of the emission spectrum at 77 K is seen to occur on a timescale comparable to that of the overall survival time of the excitations on the lattice, thus a quasi-steady-state is never achieved which results in different average lifetimes for different emission wavelengths.

We note that the particular behavior observed here, i.e., slower spectral equilibration with decrease in temperature, is not an obvious trend even within the context of the Forster weak-coupling approach. The result arises from a competition between the lack of perfect overlap, on average, between donor emission and acceptor absorption spectra, and the fact that an excitation does not have to travel far to become spectrally randomized. Both effects are due to site disorder with the former being more important.

Wavelength dependence of fluorescence lifetime of PSI whole cells

The wavelength at which the trend shifts from decreasing lifetime with decreasing temperature to increasing lifetime with decreasing temperature moves ~10 nm further to the red, i.e., from 700 to 710 nm, on going from PSI particles to whole cells of *Chlamydomonas reinhartii* A4d (see Figs. 2 *a* and 4 of Werst et al. [1992]). This may be explained by the fact that the fluorescence emission comes from all spectral types at long wavelengths (~700 nm or above). When the detection wavelength is changed from 700 to 720 nm, the contribution of the fluorescence emission from long wavelength pigments increases. Emission from these long wavelength pigments is responsible for the increase of the fluorescence lifetime. The cells contain more Chl (~120 per P700) than do the particles (~40–50 per P700) (Werst et al., 1992). If we assume that the percentage of red pigments in cells is less than that in particles, the contribution of fluorescence from red pigments in cells will be less than that in the particles at 700 nm. Thus, we expect that the

TABLE 6 **Time constants obtained from the fitting results of simulations using model 9**

		Decay parameters										
Temperature	Emission	τ_1	A_1	τ_2	A_2	τ_3	A_3	τ_4	A_4	τ_{conv}*	A_{conv}*	τ_{ave}**
K	*nm*	*ps*		*ps*		*ps*		*ps*		*ps*		*ps*
298	680	0.1	0.122	41.3	0.878					40.5	0.887	
	690	0.2	0.102	41.3	0.898					40.8	0.890	
	700	0.2	0.057	41.3	0.943					41.2	0.895	
	710	0.2	−0.042	41.3	1.042					41.3	0.900	
	720	0.2	−0.062	41.3	1.062					41.3	0.903	
77	680	3.3	0.450	14.5	0.408	48.9	0.129	132.4	0.014	10.7	0.756	15.5
	690	8.6	0.359	25.8	0.399	66.4	0.221	186.4	0.022	13.4	0.656	32.1
	700	11.2	0.116	40.0	0.553	82.3	0.296	272.1	0.035	24.1	0.441	57.4
	710	14.5	−0.393	49.2	1.087	58.3	0.243	178.7	0.063	50.7	0.525	78.7
	720	15.2	−0.551	49.7	1.348	49.8	0.153	147.5	0.051	56.8	0.509	73.7

The excitation wavelength is 654 nm. τ* and A* are the fast component and its amplitude obtained from the fit after two long lifetime components (800 ps, 7%; 4.4 ns, 4%) have been added to the decay. The decay is also convoluted with a 60-ps measured instrument function and Gaussian noise is also added. $\chi^2 \leq 1.2$.

fluorescence decay times for cells will start to increase at longer wavelengths compared with that of the particles, as is observed.

Models for energy transfer in the PSI core

In this section we briefly discuss the relationship of our model to those proposed by other workers. These models can be divided into three general classes.

(i) Kinetic schemes in which the antenna is modeled as a single species (Butler, 1975; Holzwarth, 1986, 1987, 1989 and 1991). In photosystem II such schemes have proven very valuable in elucidating the influence of charge separation and recombination processes on the fluorescence decay (Schatz et al., 1988).

(ii) Communicating box models in which the antenna is subdivided into a small number of components representing different spectral types. Within each box rapid equilibration is assumed (Wittmershaus, 1987; Mukerji and Sauer, 1988). The cluster model of Lyle and Struve (1991) is similar in spirit but in this case the cluster contains a representative sample of all spectral types. Rapid intra-cluster energy transfer is assumed.

(iii) Lattice models originally developed in analytical form by Pearlstein (1982) which consider each antenna molecule individually, and are therefore sensitive to the spatial arrangement and energies of the individual species. In principle the influence of radical pair recombination could be incorporated into this type of model, but this has not yet been done.

Clearly, the simple kinetic schemes make no comment on the role of spectral heterogeneity in the antenna. The communicating box models implicitly assume a time scale separation of the different spectral types; if, on the other hand, the different species are distributed through the protein pigment complexes such a time scale separation is not warranted. Here a distinction between the core and peripheral antennae seems appropriate. In considering the entire light harvesting apparatus a special separation of, for example, LHC proteins containing Chl *b* and Chl *a* and core proteins containing only Chl *a* seems appropriate. However, in discussing the PSI core where 80–120 Chl molecules (Zipfel and Owens, 1991) are held in a heterodimer of the *psa* A and *psa* B proteins which have putative Chl binding sites distributed throughout the sequence (there are 41 conserved histidines in *psa* A and 38 in *psa* B in eight higher plant sequences [L. Mets, private communication]), there seems no structural reason to spatially segregate different spectral types. In this context we should point out the recent confirmation (Zipfel and Owens, 1991) of our original suggestion (Owens et al., 1989) that Chlamydomonas mutant A4d has a PSI core of about half the size of the wild type.

Three representative models for the overall spectral and spatial arrangement of the antenna are the funnel model (Seely, 1973), the random model (Owens et al., 1988), and the subunit model (Causgrove et al., 1989). Our data for PSI (Werst et al., 1992), when compared with simulations, seem to rule out a funnel picture. As discussed above, models in which spectral types are placed randomly and a single low energy species is placed close to the photochemical trap are consistent with our data. The subunit model, at least in its simplest form, does not predict any wavelength dependence of the fluorescence decay because equilibration within each subunit is assumed fast, and, thus, in its simplest form is inconsistent with the data. We therefore conclude, at the present crude level of structural knowledge, that the PSI core antenna is best described by a model in which different spectral types are randomly distributed throughout the antenna. An exception to this is that a small number (one or two) of pigments of lower energy than P700 are required to reproduce the spectral and lifetime data, and these pigments must be in the near vicinity of

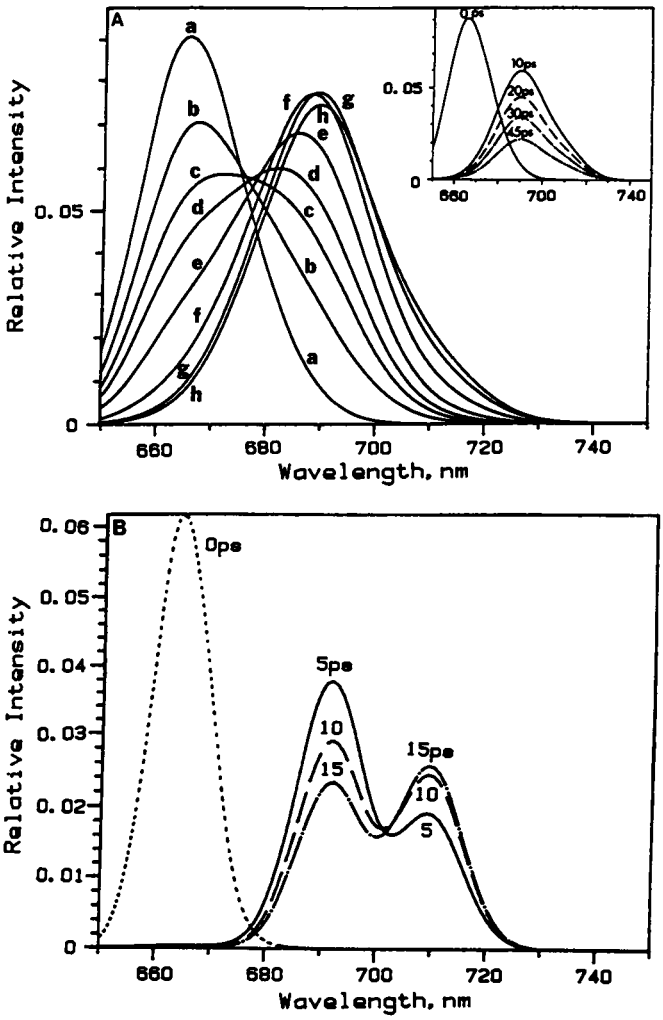

FIGURE 7 Frequency-resolved emission spectra for random model with one red pigment fixed close to the RC calculated at various times after 654-nm excitation. The spectral properties used in the calculation are according to Fig. 1. (*A*) $T = 298$ K. Spectra *a–h* are transient fluorescence emission spectra at times (ps): 0.0, 0.1, 0.2, 0.3, 0.5, 1.0, 2.0, and 3.0. The long time emission spectra shown in the upper right corner represent spectra calculated at 0, 10, 20, 30, and 45 ps. (*B*) $T = 77$ K. The spectra are shown at 0 ps (· · · · ·), 5 ps (——), 10 ps (-----), and 15 ps (— · — · —).

P700. We therefore suggest following the proposal of van Grondelle et al. (1988) for bacterial systems that such "red pigments" serve to concentrate excitation in the vicinity of the photochemical trap.

CONCLUDING REMARKS

We have investigated the role of spectral heterogeneity in energy transfer and trapping in lattice models of the PSI core antenna via self-consistent calculations of the temperature dependence of energy transfer based on Forster theory. The spatial arrangement of the chromophores is greatly oversimplified, however, the spectral characteristic is dealt with in detail and we suspect our conclusions will retain qualitative validity once more detailed structural information becomes available.

Several approximate aspects of our calculations should be improved upon. By preaveraging the inhomogeneous site broadening we focus on the role of the spectral types. This preaveraging approximation removes any wavelength dependence coming from the 200-cm^{-1} site broadening and makes the nonrandom models appear more homogeneous than they really are. The influence of dimensionality should also be considered. As the temperature is lowered and uphill transfer becomes more difficult, the number of pathways out of a pseudo-trap will become progressively more important. The relative orientations of Chl molecules are ignored in the current calculation as has the possibility of temperature dependence of the spectral position. Finally, a more realistic model for the charge separation process including the possibility of radical pair recombination should be incorporated. All these refinements can be implemented in a straightforward fashion, and will lead to much greater insight once structural informational becomes available.

The authors would like to thank Professor Laurens Mets for helpful discussions. This work was supported by a grant from NSF. Melanie Werst was the recipient of a postdoctoral fellowship from the center for Photochemistry and Photobiology at the University of Chicago and from NIH (GM14458-01).

REFERENCES

Avarmaa, R. A., and K. K. Rebane. 1982. Sharplines vibronic spectra of chlorophyll and its derivatives in solid solutions. *Chem. Phys.* 68:191–200.

Ballan, R., and E. Brezin. 1969. Nonunitary Bogoliubov transformations and extension of Wick's theorem. *Nuevo Cimento B.* 64:37–55.

Breton, J., J.-L. Martin, G. R. Fleming, and J. C. Lambry. 1988. Low-temperature femtosecond spectroscopy of the initial step of electron transfer in the reaction centers from photosynthetic purple bacteria. *Biochemistry.* 27:8276–8284.

Butler, W. L., and M. Kitajima. 1975a. A tripartite model for chloroplast fluorescence. *In* Proceedings of the Third International Congress on Photosynthesis. M. Avron, editor. Elsevier, Amsterdam. 13–24.

Butler, W. L., and M. Kitajima. 1975b. Energy transfer between photosystem II and photosystem I in chloroplasts. *Biochim. Biophys. Acta.* 396:72–85.

Causgrove, T. P., S. Yang, and W. S. Struve. 1988. Polarized pump probe spectroscopy of exciton transport in bacteriochlorophyll a protein from *Prosthecochloris aestuarii. J. Phys. Chem.* 92:6790–6795.

Fleming, G. R., J. L. Martin, and J. Breton. 1988. Rates of primary electron transfer in photosynthetic reaction centers and their mechanistic implications. *Nature (Lond.).* 333:190–192.

Forster, Th. 1965. Delocalized excitation and excitation transfer. *In* Modern Quantum Chemistry, Vol. III. O. Sinanoglu, editor. Academic Press, Inc., New York. 93–137.

Friesner, R. A., B. M. Pettitt, and J. M. Jean. 1985. Calculation of temperature-dependent multimode resonance Raman line shapes for harmonic potential surfaces. *J. Chem. Phys.* 82:2918–2926.

Gillie, J. K., G. J. Small, and J. H. Golbeck. 1989. Nonphotochemical hole burning of the native antenna complex of photosystem I (PSI-200). *J. Phys. Chem.* 93:1620–1627.

Gudowska-Nowak, E., M. D. Newton, and J. Fajer. 1990. Conformational and environmental effects on bacteriochlorophyll optical spectra: correlations of calculated spectra with structural results. *J. Phys. Chem.* 94:5795–5801.

Harris, R. A., R. A. Mathies, and W. T. Pollard. 1986. Simple interpretation of dephasing in absorption and resonance Raman theory. *J. Chem. Phys.* 85:3744–3748.

Hayes, J. M., J. K. Gillie, D. Tang, and G. J. Small. 1988. Theory for spectral hole burning of the primary electron donor state of photosynthetic reaction centers. *Biochim. Biophys. Acta.* 851:75–85.

Hemenger, R. P., K. Lakatos-Lindenberg, and R. M. Pearlstein. 1972. Incoherent exciton quenching on lattices. *J. Math. Phys.* 13:1056–1063.

Holzwarth, A. R. 1986. Fluorescence lifetimes in photosynthetic systems. *Photochem. Photobiol.* 43:707–725.

Holzwarth, A. R. 1987. Picosecond fluorescence spectroscopy and energy transfer in photosynthetic antenna pigments. *In* The Light Reactions, Vol. 8. J. Barber, editor. Elsevier, Amsterdam. 95–157.

Holzwarth, A. R. 1989. Applications of ultrafast laser spectroscopy for the study of biological systems. *Quart. Rev. Biophys.* 22:239–326.

Holzwarth, A. R. 1991. Excited state kinetics in chlorophyll systems and its relationship to the functional organization of the photosystems. *In* The Chlorophylls. H. Scheer, editor. CRC Handbook, CRC Press, Boca Raton, FL. 1125–1153.

Hsu, D., and J. L. Skinner. 1984. Nonperturbative theory of temperature-dependent optical dephasing in crystals. I. Acoustic or optical-phonons. *J. Chem. Phys.* 81:5471–5479.

Ikegami, I. 1983. Reconstitution of antenna in P-700-enriched particles from spinach. *Biochim. Biophys. Acta.* 722:492–497.

Ikegami, I., and S. Itoh. 1988. Absorption spectroscopy of P-700-enriched particles isolated from spinach. Is P-700 a dimer or a monomer? *Biochim. Biophys. Acta.* 934:39–46.

Jean, J., C. K. Chan, and G. R. Fleming. 1988. Electronic energy transfer in photosynthetic bacterial reaction centers. *Israel J. Chem.* 28:169–175.

Jean, J., C.-K. Chan, G. R. Fleming, and T. G. Owens. 1989. Excitation transport and trapping on spectrally disordered lattices. *Biophys. J.* 56:1203–1215.

Jennings, R. C., G. Zucchelli, and F. M. Garlaschi. 1990. Excitation energy transfer from the chlorophyll spectral forms to photosystem II reaction centers: a fluorescence induction study. *Biochim. Biophys. Acta.* 1016:259–265.

Jortner, J. 1976. The temperature dependent activation energy for electron transfer between biological molecules. *J. Chem. Phys.* 64:4860–4867.

Kuhlbrandt, W., and D. N. Wang. 1991. Three-dimensional structure of plant light-harvesting complex determined by electron crystallography. *Nature (Lond.).* 350:130–134.

Lyle, P., and W. S. Struve. 1991. Temperature dependence of antenna excitation transport in native photosystem I. *J. Phys. Chem.* 95:4152–4158.

Mukerji, I., and K. Sauer. 1988. Temperature dependent steady state and picosecond kinetic fluorescence measurements of a photosystem I preparation from spinach. *In* Proceedings C. S. French Symposium on Photosynthesis. Alan R. Liss, Inc. 105–122.

Munn, R. W., and R. Silbey. 1978. Ensemble averages of exponential quadratic phonon operators. *J. Phys. A. Math. Gen.* 11:939–948.

North, A. M., R. A. Pethrick, M. Kryszewski, and B. Nadolski. 1978. Solvent effects on the lowest singlet-singlet transition in chlorophyls *a* and *b*. *Acta Phys. Pol.* A54:797–804.

Owens, T. G., S. P. Webb, L. Mets, R. S. Alberte, and G. R. Fleming. 1987. Antenna size dependence of the fluorescence decay in the core antenna of photosystem I: estimates of charge separation and energy transfer rates. *Proc. Natl. Acad. Sci. USA.* 84:1532–1536.

Owens, T. G., S. P. Webb, R. S. Alberte, L. Mets, and G. R. Fleming. 1988. Antenna structure and excitation dynamics in photosystem I. I. Studies of detergent isolated photosystem I preparations using time-resolved fluorescence analysis. *Biophys. J.* 53:733–745.

Owens, T. G., S. P. Webb, L. Mets, R. S. Alberte, and G. R. Fleming. 1989. Antenna structure and excitation dynamics in photosystem I. II. Studies with mutants of *Chlamydamonas reinhardtii* lacking photosystem II. *Biophys. J.* 56:95–106.

Pearlstein, R. M. 1982. Excition migration and trapping in photosynthesis. *Photochem. Photobiol.* 35:835–844.

Pearlstein, R. M. 1991. Theoretical interpretation of antenna spectra. *In* The Chlorophylls. H. Scheer, editor. CRC Handbook, CRC Press, Boca Raton, FL. 1047–1078.

Pullerits, T., and A. Freiberg. 1991. Picosecond fluorescence of simple photosynthetic membranes: evidence of spectral inhomogeneity and directed energy transfer. *Chem. Phys.* 149:409–418.

Schatz, G. H., H. Brock, and A. R. Holzwarth. 1988. A kinetic and energetic model for the primary processes in photosystem II. *Biophys. J.* 54:397–405.

Seely, G. R. 1973. Energy transfer in a model of the photosynthetic unit of green plants. *J. Theor. Biol.* 40:189–199.

Shipman, L. L. 1977. Oscillator and dipole strengths for chlorophyll and related molecules. *Photochem. Photobiol.* 31:157–167.

van der Laan, H., Th. Schmidt, R. W. Visschers, K. J. Visscher, R. van Grondelle, and S. Volker. 1990. Energy transfer in the B800-850 antenna complex of the purple bacteria *Rhodabacter spheroides:* a study by hole burning. *Chem. Phys. Lett.* 170:230–238.

van Grondelle, R., H. Bergstrom, V. Sundstrom, R. J. van Dorssen, M. Vos, and C. N. Hunter. 1988. Excitation energy transfer in the light-harvesting antenna of photosynthetic purple bacteria: the role of the long-wavelength absorbing pigment B896. *In* Photosynthetic Light Harvesting Systems. H. Scheer and S. Schneider, editors. Walter de Gruyter & Co., New York. 519–530.

Werst, M., Y. Jia, L. Mets, and G. R. Fleming. 1992. Energy transfer and trapping in Photosystem I core antenna. A temperature study. *Biophys. J.* 61:868–878

Wilcox, R. M. 1967. Exponential operators and parameter differentiation in quantum physics. *J. Math. Phys. A.* 8:962–982.

Wittmershaus, B. P. 1987. Measurements and kinetics of picosecond time-resolved fluorescence from photosystem I and chloroplasts. *In* Progress in Photosynthesis Research. Proceedings of the 7th International Congress on Photosynthesis. Vol. 1. J. Biggins, editor. Martinus Nijhoff. 75–82.

Zipfel, W., and G. Owens. 1991. Calculation of absolute photosystem I absorption crosssections from P700 photo-oxidation kinetics. *Photosynth. Res.* 29:23–35.